Available online at www.sciencedirect.com

ScienceDirect

Procedia CIRP 142 (2026) 675–680

www.elsevier.com/locate/procedia

36th CIRP Design Conference (CIRP Design 2026)

Simplifying complex multiphase flow management through additive manufacturing-driven design exploration

Sijia Liu[a,*], Xiaoyue Ma[a], Christoph Klahn[b]

[a]Karlsruhe Institute of Technology, IMVT Institute for Micro Process Engineering, Hermann-von-Helmholz-Platz 1, 76344 Eggenstein-Leopoldshafen, Germany
[b]Karlsruhe Institute of Technology, MVM Institute of Mechanical Process Engineering and Mechanics, Geb. 30.70, 76131 Karlsruhe, Germany

* Corresponding author. Tel.: +49 721 608-24117; fax: +49 721 608-23186. *E-mail address:* sijia.liu@kit.edu

Abstract

Managing multiphase flow behavior, especially gas-liquid interactions such as bubble guiding and transport, presents significant challenges due to nonlinear interactions among geometry, interfacial forces and flow conditions. Traditional simulation-driven design methods have limitations in capturing the complex behavior of multiphase flows, particularly when tightly coupled with electrochemical kinetics and charge-mass transfer, such as in an electrolyzer. To address these challenges, this study proposes an additive manufacturing (AM)-driven experimental framework that combines rapid prototyping, a position-resolved test strategy, and a semi-quantitative scoring framework. This framework converts qualitative bubble observations into standardized, evidence-based performance metrics that correlate directly with the electrolyzer's performance. Proof-of-concept experiments conducted through representative guiding structures demonstrate that this framework reliably distinguishes between more and less effective design variants, thereby enabling iterative optimization based on experimental data. Beyond the specific case of bubble management in electrolyzer, the proposed framework establishes a transferable solution for simplifying and accelerating the structure development in complex multiphase systems.

Keywords: Additive manufacturing and optimization; Design iteration; Simplyfing complexity by AM

1. Introduction

Multiphase flows, particularly gas-liquid systems, plays an important role in numerous applications ranging from chemical processing and energy conversion to biomedical microfluidics [1–3]. Controlled guidance and release of bubbles are critical for such applications [4,5]. Taking an electrolyzer as a typical example, ineffective bubble management can lead to blockage of active electrode sites, increase ohmic resistance of the whole cell, and disrupt its flow field stability [4,5]. These factors together may result in a reduction in electrolyzer efficiency [1,6]. However, managing such flows remains constantly challenging due to the non-linear interactions between geometric structures and bubbles [7]. Even minor variations in structural features can lead to significant differences in bubble behavior, making the design of functional fluidic components complicated [7].

Traditional design methodologies rely heavily on numerical simulations to predict flow dynamics and optimize geometric structures [8,9]. Although computational models offer valuable insights, they often do not fully capture the complexity of multiphase interactions, particularly under variable real-world operating conditions [8,9]. Furthermore, simulation-based approaches are computationally costly and lack flexibility, preventing rapid iteration [8,10]. This limitation is particularly relevant when developing bubble-guided structures, which require precision, efficiency, and adaptability [4].

Recent advances in additive manufacturing (AM) provide opportunities to overcome these challenges [11,12]. This technology enables rapid prototyping of complex geometries, allowing direct experimental testing under real flow conditions [11,12]. Iterative feedback from these experiments can be integrated into subsequent design optimization, transforming development cycles into more agile and adaptive processes [12,13]. Despite its considerable potential, systematic approaches to iterative, experiment-driven design of multiphase flow components using AM remain in their exploratory phase [12].

This study proposes an AM-enabled experimental framework for multiphase flow management, integrating position-resolved testing with a semi-quantitative scoring framework directly related to bubble effects associated with electrolyzer performance. By demonstrating this framework using two representative flow-guiding structure variants, this study establishes a transferable foundation for evidence-based design of bubble guiding elements.

2212-8271 © 2026 The Authors. Published by Elsevier B.V.

10.1016/j.procir.2026.05.328

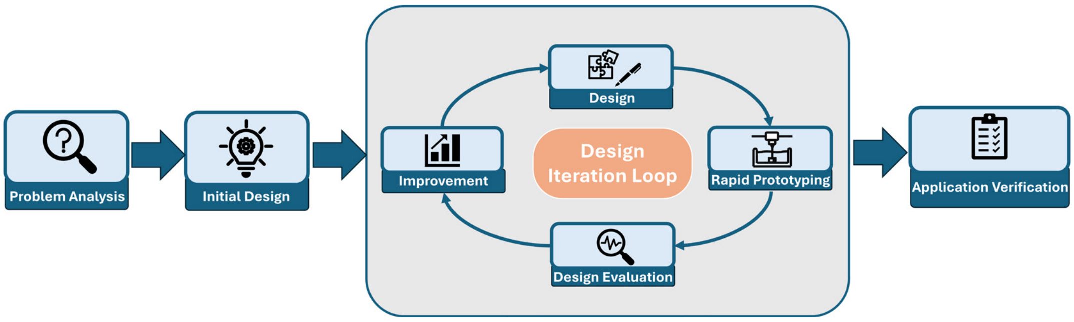

Fig. 1: Iteration Design Workflow

2. Methodology

2.1. Iterative design workflow

In conventional product and structure development, workflows often follow a V-model, where computational simulations are performed before prototyping and validation [14]. Although this method has proven its effectiveness in numerous engineering areas, its applicability is limited to bubble-guided geometries in multiphase flows [14]. This is due to the limited predictive accuracy of the simulations and the substantial computational resources required for modeling itself [4,8,10].

This limit is particularly pronounced in complex systems like electrolyzer, where bubble behavior is closely related to electrochemical reaction kinetics, electro and mass transfer, as well as electrode surface wettability [5,15,16]. Consequently, prediction methods relying solely on simulation fail to capture the multidimensional coupled effects observed in real-world scenarios [4,8,10].

This study adopts an alternative workflow that focuses on rapid prototyping and experiment-driven iteration, as illustrated in Figure 1. Instead of relying on large-scale and expensive simulations, the cycle of design - rapid prototyping – design evaluation – design optimization provides direct experimental feedback, thereby enabling efficient identification of effective and ineffective designs at an early stage and offering guidance for further iterative optimization. Importantly, the developed test set-up closely matches key boundary conditions in actual electrochemical environments, such as liquid flow velocity and bubble generation behavior, ensuring the experimental results are directly relevant to real operating environments.

2.2. Position dependent evaluation strategy

To capture the spatial heterogeneity of the multiphase flow behavior, a 3d-printed test cell was developed. It consists of a cavity with a volume of $1.00\,\mathrm{cm}^3$. The liquid inlet is located on the lower left of the cavity, while the liquid/gas outlet is located at the upper right of the cavity, as shown in Figure 2. This test unit replicates the critical boundary conditions of an electrolyzer, with flow conditions, input as well as output configurations that match those of actual commercially available flow cells [17]. Besides, the back surface of the cavity is $1.00\,\mathrm{cm}^2$ area that is uniformly subdivided into 16 regions. Each region has pore with a diameter of 1.00 mm and serves as a bubble injection site (Figure 2). This discretization models nucleation sites distributed along vertically arranged electrodes, thereby enabling position-resolved analysis of bubble behavior.

By varying the injection position under constant flow conditions, this method reveals how local geometry influences overall performance. The setup enables the decoupling of electrochemical effects whilst replicating key characteristics of the electrolytic cell, thereby allowing the interaction between bubbles and structure to be independent and underlines the necessity for local adaptive optimization.

2.3. Semi-Quantitative Scoring Framework

To systematically evaluate bubble guiding performance, a semi-quantitative scoring framework was implemented. Four indicators were selected to reflect the functional requirements in an electrolyzer and provide a reproducible basis for comparing different design iterations. More specifically:

Trajectory consistency. This metric quantifies the stability of bubble trajectories relative to the primary guiding direction, as the effective guiding structure in an electrolyzer should direct bubbles along the shortest path from their nucleation point to the flow outlet (Figure 3) [5]. For each trajectory i, the displacement vector $\Delta\mathbf{r}_i$ was compared with the desired guiding direction $\mathbf{d}$ using cosine similarity:

$$\cos\theta_i = \frac{\Delta\mathbf{r}_i \cdot \mathbf{d}}{\|\Delta\mathbf{r}_i\|\,\|\mathbf{d}\|}.$$

The mean similarity across N valid trajectories was calculated as:

$$\mu = \frac{1}{N}\sum_{i=1}^{N}\cos\theta_i,$$

and rescaled to the unit interval by $x_{\mathrm{traj}} = (\mu + 1)/2$.

Bubble area fraction. This metric assesses the proportion of electrode surface coverage, reflecting active site blockage on the electrode [16]. In each frame t, the ratio between bubble-covered area and the whole observation window was determined as $r_t = A_t/A_{\mathrm{whole}}$. Averaging over all T frames yields:

$$x_{\mathrm{area}} = \frac{1}{T}\sum_{t=1}^{T} r_t.$$

Bubble count. The average number of bubbles detected per frame was employed as a time-normalized substitute metric to evaluate the efficiency of small bubble removal.

$$x_{\mathrm{count}} = \frac{1}{T}\sum_{t=1}^{T} n_t.$$

Here, normalization by observation time ensures comparability

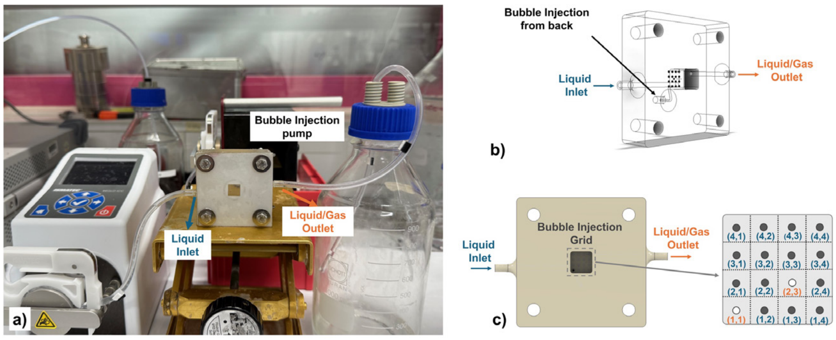

Fig. 2: Position-resolved evaluation strategy: a) Set-up for bubble behavior evaluation; b) Perspective view of 3d-printed test cell; c) Illustration of bubble injection grid

between videos of varying durations.

Macro-bubble penalty. Oversized bubbles were identified using an absolute area threshold $A_{\text{th}} = \alpha N_{\text{px}}$, with N_{px} denoting the total pixel count. For each frame t, all connected components with $A_{k,t} \geq A_{\text{th}}$ were penalized by their relative size,

$$p_t = \sum_k \frac{A_{k,t}}{A_{\text{th}}},$$

and averaged across time:

$$x_{\text{macro}} = \frac{1}{T} \sum_{t=1}^{T} p_t.$$

This metric incorporates both the frequency and persistence of large bubbles, providing a robust indicator of adverse bubble dynamics.

In addition, an **event-weighted bubble count** was implemented as an optional diagnostic metric. This variant considers bubble counts within pre- and post-event windows around macro-bubble occurrences, thereby capturing the transient response of the system. When not enabled, its weight was set to zero and the total score was not affected. When enabled, the bubble account mentioned above will be replaced by this event-weighted bubble count. This allows the overall score to reflect not only the average removal efficiency, but also captures the system's transient response during micro-bubble events.

Finally, all four indicators were converted into normalized scores to ensure comparability across different metrics. Each raw value x was scaled to the interval $[0, 1]$ as

$$\text{norm}(x; a, b) = \text{clip}\left(\tfrac{x-a}{b-a}, 0, 1\right),$$

and mapped to a 0–5 score,

$$\text{score}(x) = 5 \times \text{norm}(x; a, b).$$

For metrics where lower values are preferable (bubble area fraction, bubble count, and macro-bubble penalty), inversion was applied prior to mapping:

$$\text{score}(x) = 5 \times (1 - \text{norm}(x; a, b)).$$

The boundary values a and b correspond to the minimum and maximum values observed in all experimental datasets, respectively, ensuring uniformity of quantification across geometries. Equal weighting is used because these four metrics represent independent and equally important aspects of bubble guidance performance. The overall guidance score was then computed as the arithmetic mean of the four sub-scores:

$$S = \tfrac{1}{4}(s_{\text{traj}} + s_{\text{area}} + s_{\text{count}} + s_{\text{macro}}).$$

Equal weighting is used because these four metrics represent independent and equally important aspects of bubble guidance performance.

2.4. Fabrication and Imaging

The test geometry was fabricated using a digital light processing (DLP) printer (Asiga MAX) with commercial resin (Moiin). The printed structure was embedded into the back surface of the 3d-printed test unit described in Section 2.2 and operated under controlled fluid conditions with a bubble injection frequency of $5.00\,\text{s}^{-1}$.

Bubble dynamics was recorded via digital video. Subsequent segmentation, object detection, and trajectory analysis were performed on the image sequences using a custom Python program.

3. Proof-of-concept study

To demonstrate the feasibility of the proposed framework, a proof-of-concept study was conducted. A baseline experiment (BL) investigated bubble behavior in the 3d-printed test cell without guiding structures. Additionally, two guiding structures were incorporated within the test unit: Guiding Structure A (GS-A) and Guiding Structure B (GS-B), as illustrated in

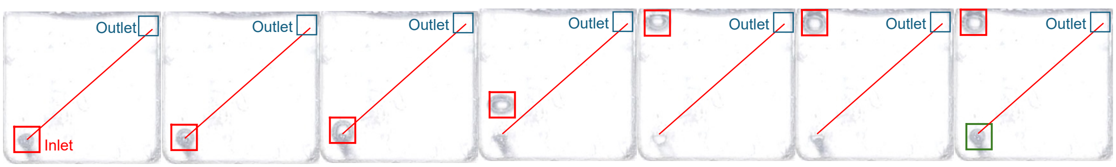

Fig. 3: Trajectory consistency: red line indicates the shortest distance between the bubble injection site and the desired outlet

Figure 4. GS-A and GS-B were selected as two representative variants of the design exploration phase, with GS-B integrating adjustments based on qualitative observations of the earlier prototype. The impact of structural modifications was evaluated by comparing the behavior of bubbles under these two structures with observations from baseline experiments.

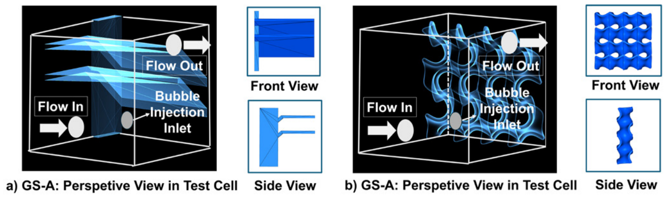

Fig. 4: a) GS-A: Perspective view, front view and side view; b) GS-B: Perspective view, front view and side view

The baseline experiment provided a reference case, capturing the dynamic behavior of bubbles in the absence of guiding elements. This experiment demonstrate that bubbles exhibit distinctly different behaviors when injected at different positions.

At position (1_1) that close to the flow inlet, bubbles detached vertically from the injection point and rose upward, gradually coalescing into large bubble. Once the big bubble reached a critical size, it migrated towards the liquid/gas outlet and was ultimately expelled from the test cell. At position (2_3) near the center of the test cell, bubbles typically followed a sequence of vertical ascent, coalescence, and eventual expulsion. However, some bubbles exhibited a backflow phenomenon, continuously coalescing before reaching the outlet and becoming trapped within the test unit. (Figure 5).

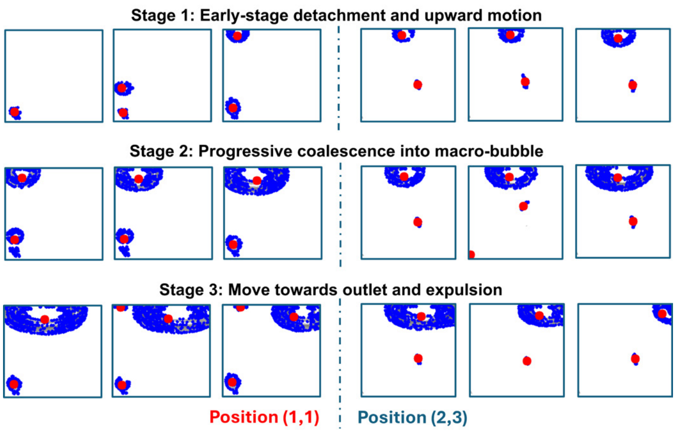

Fig. 5: Baseline experiment (BL), bubble behavior without guide structure at position position (1_1) and (2_3) separately

In contrast, when the test cell is embedded with GS-A guide structure, the bubble behavior changes significantly. Upon detachment, the bubbles were immediately laterally guided along the guiding surface, thus preventing accumulation directly above the injection site. The bubbles did not coalesce a lot, but instead traveled towards the outlet Immediately 6. At both investigation sites, bubbles were continuously removed before reaching an excessive size and no reflux phenomena were observed. This finding contrasts markedly with baseline experiments, confirming GS-A's effectiveness in promoting bubble removal.

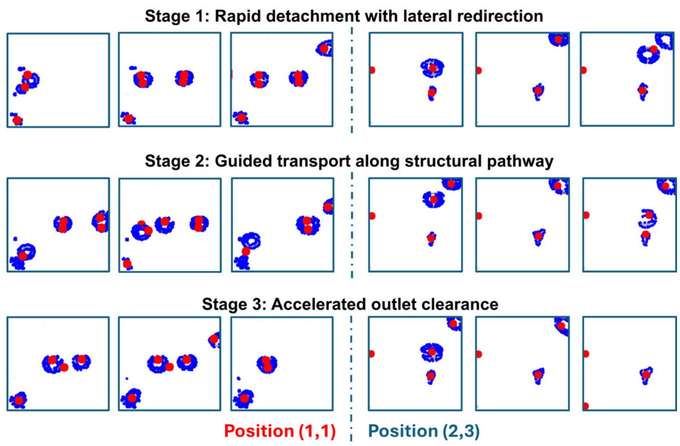

Fig. 6: Bubble guiding at position (1,1) with design geometry GS-A

In addition to GS-A, a second guide structure (GS-B) was also evaluated. This design was inspired by the streamlined characteristics of a gyroid-based blade. Due to their minimal surface properties, these geometries are frequently considered to be the preferred candidate for flow guiding element, as they provide smooth curvature and may reduce fluid flow resistance [18,19]. However, in experimental evaluations, GS-B showed only limited improvement compared to the baseline experiment without guiding elements. The observed improvement primarily manifests as a slight reduction in the retention time of macro-bubble, with a detailed quantitative analysis of this effect presented in the following section. Nevertheless, the overall injected bubble trajectories remained mostly unchanged, with macro-bubble continuing to form.

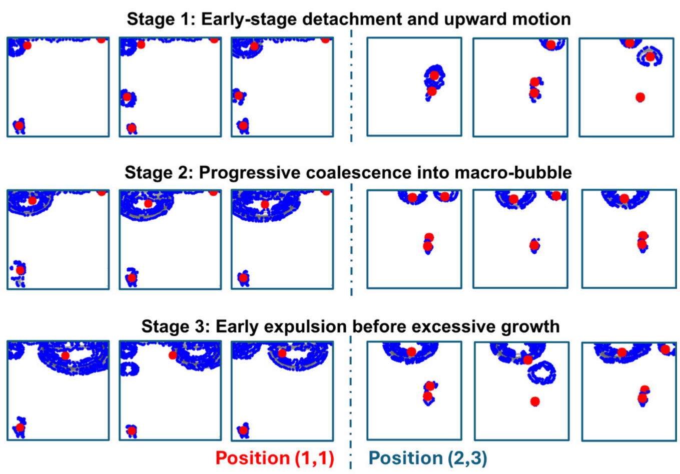

Fig. 7: Bubble guiding at position (1,1) with design geometry GS-B

In summary, the proof-of-concept experiments confirmed that the proposed framework is sensitive to structural variations. Simple guiding structure (GS-A) yielded measurable improvements, whereas more complex design (GS-B) provided only limited benefits. These findings demonstrate the framework's ability to distinguish between effective and ineffective iterations, thereby ensuring that design optimization is guided by experimental evidence rather than conceptual assumptions.

4. Application of the Semi-Quantitative Scoring Framework

Based on qualitative assessment, the semi-quantitative scoring framework proposed in Section 2.3 was applied. The selected metrics are intended to reflect the potential impact of bubbles on electrochemical performance, such as bubble detachment, transport, and the suppression of large bubbles. By converting observed dynamics into standardized numerical scores, this framework enables repeatable comparisons across design iterations. This section demonstrates its application in proof-of-concept experiments, quantifying the relative performance of the baseline structure and guided structure at representative injection locations.

The radar chart Figure 8 illustrates the semi-quantitative performance of the baseline (BL), guiding structure A (GS-A), and guiding structure B (GS-B) at two representative injection positions (1_1) and (2_3).

At position (1_1) (near the flow channel inlet), the baseline experiment demonstrated relatively high scores in bubble count and event-weighted bubble count, whilst also exhibiting a slight advantage in area fraction and trajectory consistency. This indicates that at this location, neither GS-A nor GS-B offered any significant overall improvement. However, GS-A still yielded a distinct advantage in supressing macro-bubbles, which elevated its total score despite limited benefits in other metrics, as shown in Table 1.

At position (2_3) closer to the center of the test unit, both GS-A and GS-B showed better performance than the baseline experiment, more specifically, the total score of BS was 3.12, while GS-A and GS-B achieved 3.81 and 3.41 respectively. Although the baseline experiment achieved higher scores in terms of trajectory consistency and bubble count, its average score was reduced due to frequent formation and persistent presence of macro bubbles, which is consistent with qualitative observations in Section 3. In contrast, GS-A substantially improved the bubble transport by suppressing coalescence and reducing the bubble area fraction, which is reflected in its consistently high scores across multiple metrics and the highest total score among all cases. GS-B also improved macro-bubble suppression compared to the BS, but its overall performance remained moderate due to lower scores in bubble count and trajectory consistency.

Overall, the comparison between position (1_1) and (2_3) demonstrates that the effectiveness of guiding structures is strongly position dependent. Although its benefits are limited near the inlet, it proves crucial in the middle zone where bubbles return or are trapped. Therefore, establishing a multi-criteria scoring framework is essential, as a single metric cannot comprehensively reflect the trade-offs between bubble suppression, delivery, and removal efficiency. This necessity becomes particularly pronounced when comparing different injection locations where structural performance exhibits significant difference.

Table 1: Semi-quantitative scores for baseline (BL), Guiding Structure A (GS-A), and Guiding Structure B (GS-B) at two representative injection positions.

Category	Trajectory Consistency	Bubble Area Fraction	Bubble Count	Macro-Bubble Penalty	Event-weighted Bubble Count	Total Score
BL P(1_1)	2.85	3.61	4.11	1.49	4.10	3.01
GS-A P(1_1)	2.54	3.42	2.38	5.00	2.42	3.34
GS-B P(1_1)	2.52	2.62	1.44	0.00	1.50	1.65
BL P(2_3)	4.56	3.26	4.64	0.00	4.57	3.12
GS-A P(2_3)	2.80	3.79	3.67	5.00	3.67	3.81
GS-B P(2_3)	3.07	3.63	1.94	5.00	1.77	3.41

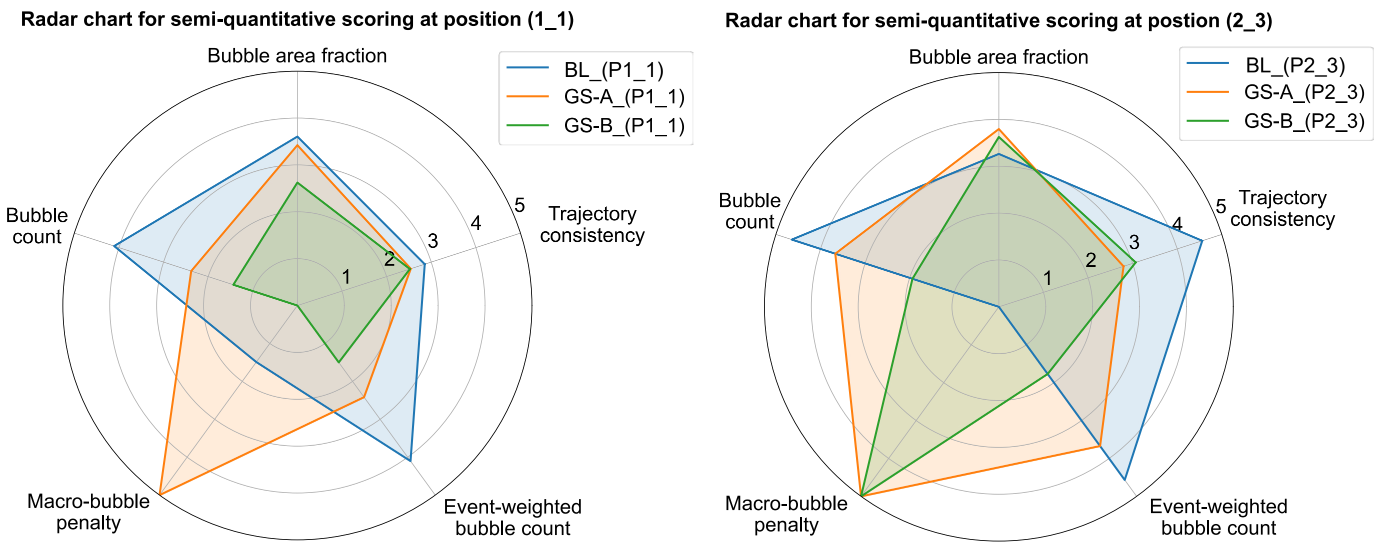

Fig. 8: Radar chart for semi-quantitative scoring at different investigated position: P (1_1) close to flow inlet; P (2_3) locates in the middle zone of test cell

5. Conclusion

This study presented a framework to simplify the management of complex multiphase flow through additive manufacturing-driven iterative exploration.. By integrating rapid prototyping with a position-resolved test strategy and a semi-quantitative scoring framework, the approach converts qualitative bubble observation into reproducible, evidence-based design feedback. The selected metrics are closely related to the functional impact of bubbles within an electrolyzer, such as the blockage of electrode active sites and current fluctuations caused by large bubbles. It ensures that the optimization targets are not only quantitative but also directly relevant to electrochemical performance.

Besides, the findings emphasize the necessity for spatially adaptive optimization of bubble-guided components, as structural effectiveness has been shown to vary across different bubbble injection locations. This highlights the need for locally tailored designs rather than uniform solutions. At the same time, this framework ensures design iterations are guided by experimental evidence rather than conceptually feasible structures.

Although the current framework has deliberately separated electrochemical reactions from interactions with geometric structures and bubbles, it provides a transferable foundation for future integration of real electrochemical conditions. Looking ahead, this approach may be integrated with Bayesian optimization, where semi-quantitative scoring serves as the objective function, thereby enabling data-driven exploration of the design space. Numerical simulation can likewise be used as an optional pre-screening or decision-support tool to identify areas of potential in the design space prior to physical prototyping, thus complementing the experiment-driven nature of the workflow. Such combinations offer a practical and scalable pathway for accelerating the development of fluid-adaptive structures within electrochemical and multiphase systems. In addition to the electrolyzer-inspired demonstration, the underlying framework can be applied to other geometry-dominated gas–liquid multiphase systems, highlighting its potential as a general design strategy for structure-dependent flow management.

Declaration of generative AI and AI-assisted technologies

By preparation of this article, the authors used ChatGPT to assist with code optimization and to improve the readability and language of the manuscript. After using this tool, the authors reviewed and edited the content as necessary and take full responsibility for the content of the published article.

Acknowledgements

The authors acknowledge the financial support by the BMFTR in the frame of the Cluster4Future ETOS by the project 'AMglass4EOS' (Grant number 03ZU1205KA)

References

[1] A. Angulo, P. Van Der Linde, H. Gardeniers, M. Modestino, D. Fernández Rivas, Influence of Bubbles on the Energy Conversion Efficiency of Electrochemical Reactors, Joule 4 (3) (2020) 555–579. doi:10.1016/j.joule.2020.01.005.

[2] L. Mei, X. Chen, B. Liu, Z. Zhang, T. Hu, J. Liang, X. Wei, L. Wang, Experimental Study on Bubble Dynamics and Mass Transfer Characteristics of Coaxial Bubbles in Petroleum-Based Liquids, ACS Omega 8 (19) (2023) 17159–17170. doi:10.1021/acsomega.3c01526.

[3] C.-T. Hsiao, J.-K. Choi, S. Singh, G. L. Chahine, T. A. Hay, Y. A. Ilinskii, E. A. Zabolotskaya, M. F. Hamilton, G. Sankin, F. Yuan, P. Zhong, Modelling single- and tandem-bubble dynamics between two parallel plates for biomedical applications, Journal of Fluid Mechanics 716 (2013) 137–170. doi:10.1017/jfm.2012.526.

[4] Y. Li, K. Li, L. Li, J. Gao, Z. Wang, W. Zou, H. Li, Q. Zhang, Y. Li, X. Zhang, D. Tian, L. Jiang, Bubble-Guidance Breaking Gas Shield for Highly Efficient Overall Water Splitting, Advanced Materials 36 (41) (2024) 2405493. doi:10.1002/adma.202405493.

[5] X. Cheng, Z.-d. Du, Y. Ding, F.-y. Li, Z.-s. Hua, H. Liu, Bubble Management for Electrolytic Water Splitting by Surface Engineering: A Review, Langmuir 39 (48) (2023) 16994–17008. doi:10.1021/acs.langmuir.3c02477.

[6] B. Ross, S. Haussener, K. Brinkert, Impact of Gas Bubble Evolution Dynamics on Electrochemical Reaction Overpotentials in Water Electrolyser Systems, The Journal of Physical Chemistry C 129 (9) (2025) 4383–4397. doi:10.1021/acs.jpcc.5c00220.

[7] Performance Enhancement of Electrocatalytic Hydrogen Evolution through Coalescence-Induced Bubble Dynamics | Journal of the American Chemical Society, https://pubs.acs.org/doi/full/10.1021/jacs.4c02018.

[8] R. Kanemoto, T. Araki, R. Misumi, S. Mitsushima, Numerical modeling of two-phase flow considering multiple bubble sizes in an alkaline water electrolyzer, Chemical Engineering Science 304 (2025) 120986. doi:10.1016/j.ces.2024.120986.

[9] K. Ekambara, K. Nandakumar, J. B. Joshi, CFD Simulation of Bubble Column Reactor Using Population Balance, Industrial & Engineering Chemistry Research 47 (21) (2008) 8505–8516. doi:10.1021/ie071393e.

[10] A. N. Jacobsen, E. Mahravan, M. V. Kragh-Schwarz, J. Catalano, P. Fooroghi, Multiphysics simulations of alkaline water electrolyzer cells — A sensitivity study on the effect of two-phase flow modeling, Electrochimica Acta 541 (2025) 147148. doi:10.1016/j.electacta.2025.147148.

[11] A. Zhakeyev, P. Wang, L. Zhang, W. Shu, H. Wang, J. Xuan, Additive Manufacturing: Unlocking the Evolution of Energy Materials, Advanced Science 4 (10) (2017) 1700187. doi:10.1002/advs.201700187.

[12] J. Plocher, A. Panesar, Review on design and structural optimisation in additive manufacturing: Towards next-generation lightweight structures, Materials & Design 183 (2019) 108164. doi:10.1016/j.matdes.2019.108164.

[13] A. Jacob, K. Windhuber, D. Ranke, G. Lanza, Planning, Evaluation and Optimization of Product Design and Manufacturing Technology Chains for New Product and Production Technologies on the Example of Additive Manufacturing, Procedia CIRP 70 (2018) 108–113. doi:10.1016/j.procir.2018.02.049.

[14] I. Graessler, J. Hentze, The new V-Model of VDI 2206 and its validation 68 (5) 312–324. doi:10.1515/auto-2020-0015.

[15] J. Bleeker, C. van Kasteren, J. R. van Ommen, D. A. Vermaas, Gas bubble removal from a zero-gap alkaline electrolyser with a pressure swing and why foam electrodes might not be suitable at high current densities, International Journal of Hydrogen Energy 57 (2024) 1398–1407. doi:10.1016/j.ijhydene.2024.01.147.

[16] H. Rox, A. Bashkatov, X. Yang, S. Loos, G. Mutschke, G. Gerbeth, K. Eckert, Bubble size distribution and electrode coverage at porous nickel electrodes in a novel 3-electrode flow-through cell, International Journal of Hydrogen Energy 48 (8) (2023) 2892–2905. doi:10.1016/j.ijhydene.2022.10.165.

[17] E. Heeschen, E. DeLucia, Y. Arin Manav, D. Roberts, B. Davaji, M. H. Barecka, Low cost 3D printable flow reactors for electrochemistry, HardwareX 17 (2024) e00505. doi:10.1016/j.ohx.2023.e00505.

[18] W. Tang, C. Zou, H. Zhou, L. Zhang, Y. Zeng, L. Sun, Y. Zhao, M. Yan, J. Fu, J. Hu, Z. Li, Z. Liu, T. Wang, Z. Zhang, A novel convective heat transfer enhancement method based on precise control of Gyroid-type TPMS lattice structure, Applied Thermal Engineering 230 (2023) 120797. doi:10.1016/j.applthermaleng.2023.120797.

[19] K. Yeranee, Y. Rao, Turbulent Flow and Heat Transfer Enhancement for Turbine Blade Trailing Edge Cooling With Gyroid-Type Triply Periodic Minimal Surfaces, Journal of Engineering for Gas Turbines and Power 145 (071008) (Apr. 2023). doi:10.1115/1.4062157.